Possible Bounds on the Earth's Surface Temperature: From the Perspective of a Conceptual Global-Mean Model*

HSIEN-WANG OU

Lamont–Doherty Earth Observatory, Columbia University, Palisades, New York

(Manuscript received 6 April 2000, in final form 8 December 2000)

ABSTRACT

A global-mean model is used here to elucidate possible bounds on the surface temperature of a simplified ocean–atmosphere system. Extending previous one-dimensional models, it has included as internal variables the low-level and high-level cloud covers and the turbulent wind at the surface. The main hypothesis for the model closure is that the conversion rate from the solar to the kinetic energy—or, equivalently, the rate of internal entropy production—is maximized, which has been applied with considerable success in past latitudinal models. From the model derivation, it is found that the surface temperature is narrowly bounded below by the onset of the greenhouse effect and above by the rapid increase of the saturation vapor pressure. Because both are largely intrinsic properties of water, the resulting surface temperature is mostly insensitive to detailed balances or changing external conditions. Even with a 50% change of the solar constant from its present-day value, the model temperature has varied by only about 10 K. The reason that the heat balances can be maintained is an internal adjustment of the low cloud cover, which offsets the solar effect. The model offers a plausible explanation of an equable climate in the geological past so long as there is a substantial ocean.

1. Introduction

A climate not unlike the present-day one has prevailed on the earth since its early history when the sun was considerably dimmer (e.g., Crowley and North 1991). How the earth maintains this climate is a matter of speculation, and many possible scenarios have been suggested. The most widely circulated among them is a much higher concentration of carbon dioxide (CO_2) in the atmosphere, which has been attributed to external factors, though poorly constrained by observational data. Also suggested but less explored is a reduced cloud albedo that may offset the solar effect. Since there are no proxy data for the cloud cover, which in addition is an internal variable, this possibility may be assessed only through a model that has included interactive cloud covers. Conversely, without a physical closure that contains variable clouds—which directly affect the energy flow into the system—one simply does *not* have an explanation of the earth's temperature. It is the desire to formulate such a model to try to address this ''faint young sun'' paradox that motivates the current study.

In terms of relevant studies, it should first be pointed out that, although variable clouds have been incorporated in some GCMs (see chapter 7 of Liou 1992), these models provide little guidance to the above problem since the relevant parameters (such as the threshold relative humidity for cloud formation) are often tuned to yield the observed cloud covers. It should also be remarked that, while there is an extensive and rapidly growing body of literature on various feedback processes when the present-day climate is perturbed—for example, by the doubling of the atmospheric CO_2, it is the *basic* state itself that is of concern. That is, while many of these processes are demonstrably important for small climate changes, they may not be the deciding factors that give rise to the earthlike climate. Clearly, to address questions as crude as an ''earthlike'' climate, it suffices to consider a minimal global-mean that retains only dominant balances.

While there are many one-dimensional models that address various aspects of the climate problem, two are particularly relevant to the current study, because they share the explicit aim of determining the earth's temperature from first principles. One is that of Sarachik (1978), who applied his model to the Tropics by neglecting its heat exchange with the subtropics, a coupling that has taken on an increasingly important role in recent studies (Hartmann and Michelsen 1993; Pierrehumbert 1995). In addition, his model contains no clouds and the turbulent wind is specified, both of which impose considerable limitations on the model. In contrast, Paltridge (1974) applied his one-dimensional mod-

* Lamont–Doherty Earth Observatory Contribution Number 6131.

Corresponding author address: Hsien-Wang Ou, Lamont–Doherty Earth Observatory, Columbia University, Palisades, NY 10964.
E-mail: dou@ldeo.columbia.edu

el to the global-mean fields, thus bypassing the above difficulty of meridional fluxes. The trade-off, however, lies in the uncertainty in interpreting the model temperature, since the observed temperature varies from equator to pole and enters the global balances nonlinearly. One major advance of Paltridge is the inclusion of a variable cloud cover, which, as remarked above, is among the most important climate variables. For simplicity, however, his cloud cover is represented by a *single* variable, with no provisions made for low-level and high-level clouds, which affect global balances in fundamentally different ways. In terms of its logical development, the current model represents a step beyond Paltridge (1974) by including as internal variables both low-level and high-level cloud covers (hereinafter referred to as ''low cloud cover'' and ''high cloud cover'') and the turbulent wind velocity. But, perhaps more important, the additional degrees of freedom introduced by these variables allow a model closure based on an extremization principle, as discussed next.

Scientists have long been puzzled by the inefficiency of the earth's atmosphere as a heat engine, which converts only a few percent of the absorbed solar energy to kinetic energy (Lorenz 1967). For lack of physical explanations, Lorenz (1960) speculated that this conversion rate is the maximum allowed, without specifying just what properties of the climate system may impose such a bound. Since, in a steady state, this converted energy is wholly dissipated by irreversible processes, Lorenz's hypothesis is equivalent to the maximization of internal entropy production, a proposition that has been independently explored by Paltridge (1978) and extensively discussed in the literature (e.g., Mobbs 1982). One general argument for such thermodynamic principles is that—paraphrasing Paltridge (1978)—when a system contains more degrees of freedom than can be practically constrained, it would settle down (i.e., steady state) only when some thermodynamic properties are extremized. In an isolated system, this is the well-known second law of thermodynamics, which maximizes the entropy. In an open system that exchanges energy with the surrounding, it is the entropy production rate that is extremized. In fact, under certain conditions, though not likely met by a climate system (Essex 1984), it could be shown that the internal entropy production is minimized in the steady state (see De Groot and Mazur 1963). Although Lorenz (1960) and Paltridge (1979) have devised possible scenarios for the maximization of the internal entropy production, for lack of rigorous derivation, it should be regarded as a working hypothesis whose support derives mainly from its successful applications.

This maximization principle has been applied in its many equivalent forms. Since in a steady state the entropy production rate equals the generation rate of the available potential energy, Schulman (1977) used the latter to determine the meridional distribution of temperature, which compares favorably with observation. Since his model contains no dynamics, the startling implication is that the large-scale circulation is subsumed by thermodynamics in the distribution of temperature. Similarly, since a maximization of the internal entropy production implies a minimized entropy exchange with the surroundings (there could be no change of entropy in the steady state), Paltridge (1978) used the latter to determine the latitudinal distribution of surface temperature and cloud cover and met with considerable success, further underscoring the thermodynamic nature of the system.

Since such extremization principles, if operative, are properties of a dissipative thermodynamic system, they should be equally applicable to vertical as to latitudinal models. This is reflected in the above-cited arguments, which made no reference to spatial dimensions of the system. It is the use of such an extremization principle that particularly distinguishes the current model from previous one-dimensional models, which, as we shall see later, invariably leads to a more stable climate (see section 4). For its specific implementation, one notes that, in a steady state, the rate of internal entropy production equals the rate of kinetic energy dissipation (Schulman 1977) and that the latter is dominated by the surface friction acting on the turbulent wind [see Fig. 2.4 of Garratt (1992) and Fig. 14.8 of Peixoto and Oort (1992), the latter referred to hereinafter as PO92]. In accordance, it is assumed that *the turbulent wind at the surface is maximized.* As we shall see later, the turbulent wind enters global balances through surface fluxes of sensible and latent heat, and its maximization allows the selection of a particular solution out of the whole family of solutions that is consistent with global balances.

For the organization of the paper, I shall first describe in section 2 the simplified ocean–atmosphere system that is considered. The physical closure is formulated in section 3, through which the surface temperature is determined, and its dependence on a changing solar constant examined. The paper is concluded in section 4 by further discussion.

2. Model system

As discussed above, the aim is to examine the consequence of a well-known thermodynamic principle when applied to a global-mean model and to see whether it may explain an earthlike temperature. To address such crude questions, I consider a minimalistic model containing only dominant balances, which serves to reveal the essential physics in a more transparent manner. Since the essence of the theory lies in its closure, the neglect of lesser terms can be justified if it does not alter this closure to pose a serious limitation on the theory. Moreover, as it turns out, the model temperature is narrowly constrained by intrinsic properties of water and hence is insulated from detailed balances. This robustness is further affirmed when some neglected terms are includ-

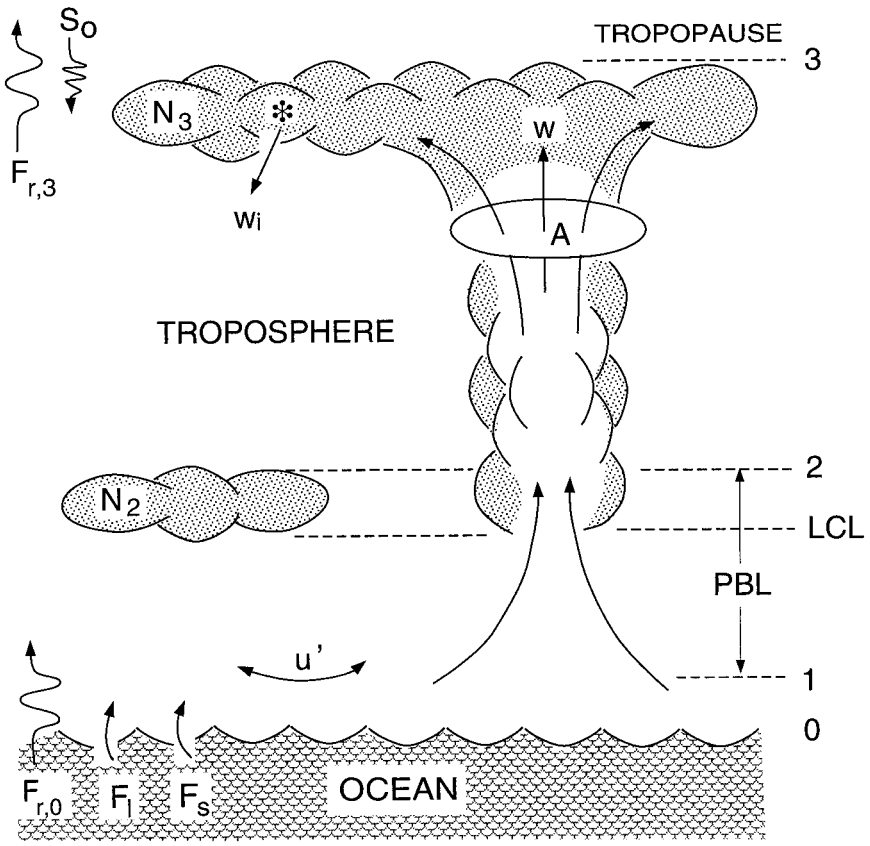

FIG. 1. A schematic of the model system. Levels 0, 1, 2, and 3 mark, respectively, the ocean surface, the top of the air–sea interfacial layer, the top of the low clouds, and the tropopause. Because of the shallowness of the low clouds, no distinction in height is made between level 2 and the LCL. Variables with a numerical subscript indicate global means at the respective level, which may differ from their values in the updrafts. The symbols A, N_2, N_3 indicate fractional areas occupied by the deep updrafts, the low, and high clouds, respectively; u' is the turbulent wind velocity at level 1; and w and w_i are the vertical velocities of the deep updrafts and the settling ice (both taken as positive), respectively. Other symbols are defined in the text.

ed in the calculation and have produced no appreciable change in the surface temperature (see later discussion). In any event, since the solar constant has varied over a wide range (by threefold) in the calculations, it most likely has outpaced all the neglected effects.

With these caveats in mind, I consider an ocean–atmosphere system sketched in Fig. 1. It is heated by shortwave (SW) radiation from the sun, which, other than being reflected by clouds, is wholly absorbed by the ocean. The ocean warms the atmosphere through longwave (LW) radiation and fluxes of sensible and latent heat, the latter two effected by the turbulent wind. The latent heat is released when moisture in the rising air is condensed, forming clouds, and reenters the ocean through precipitation. The heat exits the system through the outgoing longwave radiation (OLR), which completes the circuit.

Updrafts are initiated when the surface air has acquired the temperature of the warmer ocean surface and rises. Since the rising air retains the specific humidity of the ambient, it is undersaturated and cools off dry adiabatically until it is saturated, which marks the lifting condensation level (LCL) and the cloud base. While the above property distributions in the updraft are invoked in the model derivation, they do not affect the global-mean fields on account of the (assumed) small areal coverage of the updrafts.

Distinction is further made between shallow updrafts capped by the low clouds and deep updrafts extending to the tropopause where the high clouds lie. The defining character of the shallow updrafts is that their buoyancy is derived solely from the surface sensible heat flux and hence may be consumed by the cloud-top cooling. The top of the low clouds thus caps the shallow updrafts, which defines the planetary boundary layer (PBL). Examples of low clouds include vast sheets of low stratus in the Arctic and over eastern subtropical oceans (Hartmann et al. 1992). Their shallowness has been attributed to large-scale subsidence (Sarachik 1978) or entrainment induced by cloud-top cooling (Liou 1992), which brings in the dry air from above to dissipate the clouds.

Because of this shallowness of the cloud top, no distinction is made between its height and the LCL.

The deep updrafts, on the other hand, are conduits of the upward transport of vapor flux derived from surface evaporation. Through condensation, the excess moisture provides a continual source of buoyancy that propels the deep updrafts to the tropopause. For this reason, the deep updrafts are the main sites of precipitation, and water condensates that do not precipitate locally would be carried by the outflow to form high clouds. Examples of high clouds include cirrus bands over the intertropical convergence zone and midlatitude storm tracks, which are indeed sites of surface convergence of moisture and maximum precipitation. Being a manifestation of the outflowing air at the tropopause, cirrus are typically thin (Borovikov et al. 1963); their vertical dimension thus is neglected for simplicity. Although the core of the deep updrafts contains cumulonimbus clouds, their radiative effects on global balances are neglected on account of their small areal coverage.

While this classification of clouds into low clouds at the LCL and high clouds at the tropopause represents an extreme simplification, it is nevertheless consistent with the observed bimodality in the cloud amounts [see Fig. 4.6 of Liou (1992)]. As discussed next, the two cloud types have very different radiative properties; their incorporation thus represents a significant improvement over Paltridge's (1974) single-cloud-layer model. Readers are referred to Liou (1992) and Webster (1994) for a detailed discussion of cloud radiative properties. For my purpose, it suffices to note that the low clouds have high water density and hence are effective in both reflecting SW flux and emitting LW flux. The high clouds, on the other hand, have very low water density and hence small albedo, but, because they are composed of ice crystals, they remain strong thermal emitters. By incorporating only the *dominant* effects, it is assumed therefore that the low clouds have unit albedo, that the high clouds are transparent in the SW band, and that both clouds are black in the LW band.

One notes that deviations from unit albedo or emissivity can be partly accommodated by interpreting the model cloud covers as effective ones, which thus pose *no* limitation on the theory. More serious, perhaps, is the neglect of the high cloud albedo, which could be substantial in the Tropics (Ramanathan and Collins 1991). However, I am concerned with global-mean properties, and albedo of the high clouds is neglected *in comparison with* that of the low clouds. The fact that high clouds are less visible than low clouds in the SW band provides anecdotal support of this approximation [see, e.g., Figs. 4.1–4.3 of Liou (1992)]. More quantitative, if one uses an ice-water density of 10^{-2} g m^{-3} [Fig. 4.13 of Liou (1992)] and a thickness of 1 km for a typical cirrus, its ice-water path is 10 g m^{-2}, which would yield an albedo of less than 0.2 according to Fig. 5.25 of Liou (1992). This value is considerably smaller than the albedo of low clouds, which has a value in the high tenths. The inclusion of the high-cloud albedo would complicate the mathematical derivation (straightforward nonetheless), and using the above value of 0.2 has produced no appreciable change in the surface temperature (less than 1 K), which further justifies its neglect.

For the radiative properties of the clear sky, one may assume, to good approximation, that water vapor is the only greenhouse gas. Since water vapor is confined to the troposphere, the radiative balance above the tropopause implies that the latter is at the skin temperature, a function only of the absorbed solar flux. For an observational check of this deduction, one may use a planetary albedo of 0.3 to yield a skin temperature of 215 K, which lies within the observed range of the tropopause temperature (see Fig. 7.5 of PO92). In the model, the low cloud cover, however, is a calculated property, and hence the tropopause temperature is as well, and, being the emitting temperature of the high clouds, it enters the global heat balances.

For the model closure, one also needs to know the clear-sky LW fluxes, which depend on the ocean surface temperature, and the vertical distributions of temperature and vapor pressure in the atmosphere. The latter two may be assumed functions of only the former based on the following observations: 1) the air–sea temperature difference is small (see Fig. 10.7 of PO92), a condition that can additionally be checked a posteriori since this temperature difference is calculated in the model (see section 3d); 2) the lapse rate is moist adiabatic (Ramanathan and Coakley 1978); and 3) the relative humidity is mainly a function of height (see Fig. 12.4 of PO92). As a consequence, the clear-sky LW fluxes at the surface and the tropopause are functions only of the surface temperature. Note that these assumptions form the basis of many radiative calculations, including those of Hartmann and Michelsen (1993) and Pierrehumbert (1995), which provide the LW fluxes used in the current model. These assumptions, in total or in part, have also been invoked in many climate change studies, even though such studies demand far greater accuracy than this model. A fixed relative humidity profile, for example, was used in early radiative–convective models (e.g., Manabe and Wetherald 1967). In support of its usage, it has also emerged as a robust feature in models that have explicitly included the hydrological cycle (Cess et al. 1990; Clement and Seager 1999), and heuristic arguments as to why this should be the case have been given by Held and Soden (2000). In any event, since the aforementioned LW fluxes are not particularly sensitive to the relative humidity of the surface air, the model solution does not hinge heavily on this assumption. Lest one should falsely interpret the observation, it is emphasized that I am concerned with the vertical distribution of the *global-mean* fields, which may differ from that of the *local* fields, such as that in the updrafts (as discussed earlier) or frontal zones (Stone and Carlson 1979). Because the above temperature and humidity

distributions are assumed, rather than derived, the theory obviously is fundamentally incomplete.

3. Model formulation

As sketched in Fig. 1, levels 0, 1, 2, and 3 are used to designate, respectively, the ocean surface, top of the air–sea interfacial layer, top of the low clouds, and the tropopause. Variables with these numerical subscripts are global means at the respective level, which may differ from their values in the updrafts. For simplicity, all variables, unless otherwise stated, are henceforth nondimensionalized. To be specific, all the heat fluxes have been scaled by $S_0 \approx 340$ W m^{-2} (one-quarter of the present-day solar constant), temperature T has been scaled $(\sigma^{-1}S_0)^{1/4} \approx 279$ K (σ being the Stefan–Boltzmann constant), and the blackbody radiance B has been scaled by $\pi^{-1}S_0$. For simplicity, it is assumed from the outset that differences between T_0, T_1, and T_2 are sufficiently small that

$$B_0 \approx B_1 \approx B_2. \tag{1}$$

In the present-day climate, these temperatures differ by less than 10 K, so the approximation holds to within about 10%. In any event, since these temperatures are calculated in the model, the above approximation can be checked a posteriori for consistency (section 3d).

The derivation of the surface temperature proceeds as follows. I first treat this temperature as an independent variable and, through global balances, calculate other climate variables, such as the low and high cloud covers and the turbulent wind, as functions of this temperature. It turns out that the turbulent wind has a distinct maximum, which then specifies the surface temperature, in accordance with the model hypothesis. It is convenient that the approximations used in the model allow the above climate variables to be determined successively; the model derivation thus is presented in this same manner.

a. Low cloud cover

The following derivation seeks to relate the low cloud cover to the surface temperature, and it consists of three basic steps: the heat balances at the surface and the top of the low clouds, and the linkage of the latent to the sensible heat flux at the surface.

I begin with the heat balance at the surface, given in dimensionless form,

$$1 - N_2 = F_s + F_l + (1 - N_2)F_{r,0}, \tag{2}$$

where N_2 is the low cloud cover; F_s and F_l are the sensible and latent heat fluxes, respectively; and $F_{r,0}$ is the (net upward) clear-sky LW flux, given by

$$F_{r,0} = B_0 - F_0^-, \tag{3}$$

in which the sign of the superscript signifies the direction of the flux (negative for downward). In (2), I have neglected the SW albedo of the high clouds, as discussed in section 2. I have also neglected the net LW flux under the low clouds, which is of the form $N_2[B_0 - (1 - \varepsilon')B_2 - \varepsilon' B_{\text{PBL}}^-]$, where ε' is the emissivity of the PBL and B_{PBL}^- signifies the downward blackbody radiance of this layer. This last expression simply states that this flux is a difference between upward and downward fluxes, the latter consisting of the transmitted cloud radiation and that emitted by the PBL. Since ε' is less than unity, and B_{PBL}^- lies between B_0 and B_2, this flux is thus small on account of (1). I have also neglected in (2) the downward LW flux from the high clouds, which has the form $N_3(1 - \varepsilon)B_3$, if not blocked by the low clouds. In this expression, N_3 is the high cloud cover, ε is the emissivity of the troposphere, and B_3 is the blackbody radiance of the high clouds, which, as discussed in section 2, are at the skin temperature, or

$$B_3 = (1 - N_2)/2. \tag{4}$$

In the present-day climate, the troposphere is practically opaque to the downward LW flux except in the spectral window that makes up about 30% of the blackbody radiance, or $1 - \varepsilon \leq 0.3$. Considering the appearance of other multiplication factors, which are all less than one, and a possible blockage of this flux by the low clouds, it is small when compared with unity and hence is neglected.

I shall next consider the heat balance at the level of the low-cloud top (level 2), which, as discussed in section 2, approximately aligns with the LCL. Because the latent heat is not released below the LCL, the turbulence that defines the PBL derives its energy mainly from the sensible heat flux from the surface. The bulk of this energy is dissipated by the surface friction, with a small leftover expended to entrain air from across the stable upper boundary (the inversion). In other words, the buoyancy flux at the LCL is a small fraction (and opposite in sign) of its surface value. This fraction is about 0.2 for dry convection based on empirical evidence (Deardorff et al. 1969), although it could be larger if the PBL is topped by clouds because of the additional energy source provided by the cloud-top cooling (Deardorff and Businger 1980). Now that the sensible heat flux is proportional to the buoyancy flux (if one neglects the small virtual effect), its magnitude at level 2 thus is small when compared with its surface value, which itself is small, and hence may be neglected. One may opt to retain this small sensible heat flux at the LCL, as done in Sarachik (1978) or Betts and Ridgway (1989), which however does not change the model result in any significant way, but would introduce a highly uncertain empirical parameter.

If one neglects also the downward LW flux from the high clouds, as discussed earlier, the heat balance at level 2 is approximately

$$1 - N_2 = F_l + N_2F_{e,2} + (1 - N_2)F_{r,2}. \tag{5}$$

Note that the latent heat flux has maintained its surface

value since there is no condensation below the LCL (neglecting also evaporation of precipitation in the PBL). In the above equation,

$$F_{e,2} = B_2 - F_2^- \tag{6}$$

is the ''effective'' radiation of the low clouds on account of their thermal blackness, and

$$F_{r,2} = F_2^+ - F_2^- \tag{7}$$

is the net clear-sky LW flux, with

$$F_2^+ = (1 - \varepsilon')B_0 + \varepsilon' B_{\mathrm{PBL}}^+, \tag{8}$$

following earlier notations (i.e., ε' is the emissivity of the PBL, and B_{PBL}^+ is the upward blackbody radiance of this layer). Equation (8) states that the upward clear-sky LW flux (at level 2) consists of that transmitted from the surface and that emitted by the PBL. Again, since emissivity ε' is less than unity and B_{PBL}^+ lies between B_0 and B_2, the difference between $F_{e,2}$ and $F_{r,2}$ is bounded by $B_0 - B_2$ and hence is negligible on account of (1). By substituting this approximation

$$F_{e,2} \approx F_{r,2} \tag{9}$$

into (5), the latter is simplified to

$$1 - N_2 = F_l + F_{r,2}. \tag{10}$$

One notes that because the low clouds have a similar emitting temperature as the ocean surface, they do not enter this equation. For a further simplification, $F_{r,2}$ in (10) will be replaced by $F_{r,0}$, based on the following considerations. The difference of the two, of course, represents the clear-sky cooling of the PBL, and, although it is not as small as $F_{r,2} - F_{e,2}$ (since the air above the PBL is very dry), it may remain small because of the strong absorption. Based on observations, the local cooling rate of the PBL is on the order of 1 K day^{-1} [see, e.g., Fig. 6.28 of Liou (1992)], and, with a height of 1 km, the PBL as a whole is cooled at a rate on the order of 10 W m^{-2}, which is small when compared with the net LW flux (on the order of 100 W m^{-2}) and hence is neglected in (10). With the approximation

$$F_{r,2} \approx F_{r,0}, \tag{11}$$

(10) becomes

$$1 - N_2 = F_l + F_{r,0}, \tag{12}$$

which states that the SW flux on the lhs is balanced on the rhs by the latent heat and net LW fluxes, both of which are approximated by their surface values.

The heat balances at the surface [(2)] and the cloud top [(12)] can now be combined to yield

$$F_s = N_2 F_{r,0}, \tag{13}$$

which states that the sensible heat flux from the surface is expended by the cloud-top cooling. To explain this physically, one notes that the absence of the latent heat release in the PBL implies that radiative cooling of the layer is balanced by the sensible heat flux. Now that the sensible heat flux across its upper boundary and the radiative cooling of the layer in the clear sky are both small, one is led immediately to (13). For a cursory check of (13) from observations, one may use $N_2 \approx 0.3$ and $F_{r,0} \approx 100$ W m^{-2} to yield $F_s \approx 30$ W m^{-2}, which is on the right order of the observed value. It is also worth mentioning that, since the cooling rate under the clouds is highly skewed toward the cloud top [e.g., Fig. 13.2 of Emanuel (1994)], the low clouds play the dual roles of enhancing the buoyancy flux below the clouds, as alluded to earlier, and depleting it at the cloud top.

Having expressed the sensible heat flux in terms of the low cloud cover [(13)], I now proceed to constrain the latent heat flux. The two heat fluxes are related by definition through the Bowen ratio Bo,

$$F_l = \mathrm{Bo}^{-1} F_s. \tag{14}$$

We shall next argue that Bo may be approximated by its saturation value, a function thus only of the surface temperature. Using the bulk aerodynamic formulas for the two fluxes (see PO92), one obtains

$$\mathrm{Bo}^{-1} = \frac{1}{\gamma}\frac{e_0 - e_1}{T_0 - T_1}, \tag{15}$$

where $\gamma \equiv (0.622L)^{-1} c_p p_0$ is the Bowen constant (L is the latent heat of vaporization, c_p is the specific heat, and p_0 is the pressure at the ocean surface), and $e_0 = e_s(T_0)$ is the saturation vapor pressure e_s at the ocean temperature T_0. As seen later (section 3c), the maximization principle used in the model implies that Bo be maximized (or Bo^{-1} minimized); e_1 thus should approach its saturation value. As we have noted in section 2, however, the air in the updrafts is undersaturated near the surface; the global-mean relative humidity of the surface air thus is less than 100%, the deviation being related to the fractional area of the updrafts. Let this area be denoted by A_1; a crude derivation (appendix A) shows that

$$\mathrm{Bo}^{-1} = (1 - A_1)^{-1}\mathrm{Bo}_s^{-1}, \tag{16}$$

where Bo$_s$ is the saturation value given by

$$\mathrm{Bo}_s^{-1} = \frac{1}{\gamma}\frac{de_s}{dT}. \tag{17}$$

There may not be a definite value for A_1 except that it is generally assumed to be small (see section 2). I shall therefore approximate the maximized Bowen ratio by its saturation value

$$\mathrm{Bo} \approx \mathrm{Bo}_s, \tag{18}$$

which is a known function of the surface temperature. There exist, of course, empirical formulas for Bo (e.g., Garratt 1992), which could deviate significantly from the saturation value. This, however, may partly reflect the difference between local conditions (e.g., in the updrafts) and the mean condition of relevance here (not to mention idealization of the model system). Given that

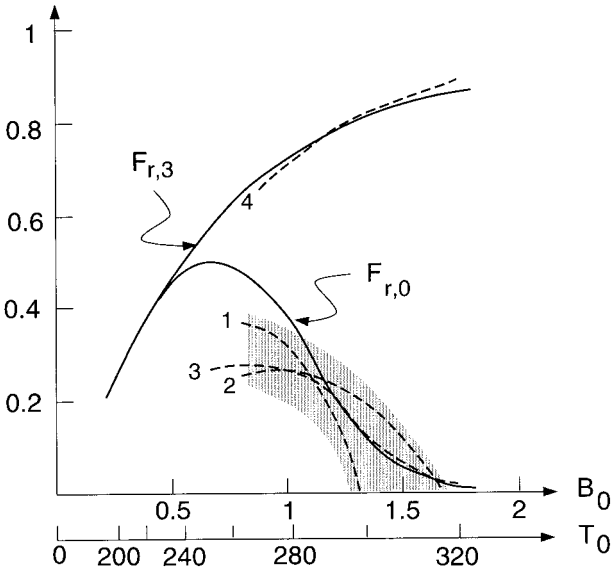

FIG. 2. Radiative fluxes used in the model (solid lines), as compared with that calculated by Hartmann and Michelsen (1993, line 3) and Pierrehumbert (1995, line 4). Also plotted are curves based on Brunt's empirical formulas [see Kondratyev (1969), his Eq. (9.44) and Table 9.10, setting the surface relative humidity to 80%]: line 1 from Robitsch (1934, Germany) with $a = 0.66$ and $b = 0.127$; and line 2 for Chumakova (1947, Karadag) with $a = 0.376$, $b = 0.043$. Lines 1 and 2 roughly span the range of empirical values, which is shaded.

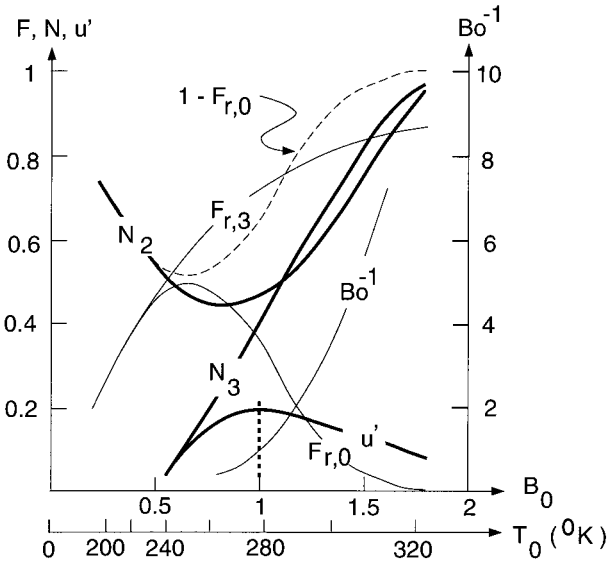

FIG. 3. Calculated values of the global-mean fields (thick solid lines) as functions of the surface temperature. Thin solid lines are specified functions. The maximum in u' specifies the surface temperature, in accordance with the model hypothesis.

the empirical formulas contain uncertain parameters [e.g., the factor α in Garratt (1992)] and that, as seen later, they would not alter the model conclusion in significant ways, their use is deemed less desirable than the approximation in (18).

With the approximation of (18), the latent heat flux can be expressed in terms of the low cloud cover through (14) and (13), and, when this expression is substituted into (12), one finally arrives at

$$N_2 = (1 - F_{r,0})(1 + \mathrm{Bo}_s^{-1} F_{r,0})^{-1}, \qquad (19)$$

which allows the calculation of N_2 as a function of the surface temperature once $F_{r,0}$ is specified. The latter, as alluded to in section 2, is based on values calculated from radiative transfer equations. To be specific, Hartmann and Michelsen's curve (1993, line 3 in Fig. 2) is fitted by a low-order analytical function of the form

$$F_{r,0} = B_0 \exp(-aB_0^b) \qquad (20)$$

by tuning coefficients a and b. This analytical form assures that $F_{r,0} \approx B_0$ as $B_0 \to 0$, as it should be with the vanishing of the greenhouse effect. Given the low-order form, I have chosen to fit the curves more closely where there is a rapid decrease of the flux (or increase of the greenhouse effect), which, as seen later, is an important feature in constraining the model temperature. For comparisons, I have also plotted two radiative curves based on Brunt's empirical formulas (lines 1 and 2, see caption of Fig. 2 for the specifics). The two curves are chosen because they roughly span the range of empirical values, which is as shaded. It is seen that the model curve is higher than the dashed curves at low temperatures, which could be justified by the following considerations. First of all, it is seen from the derivations that we have used $F_{r,0}$ to approximate $F_{r,2}$; the latter could be significantly greater at low temperatures (as the air above the PBL becomes more transparent). Second, the empirical curves likely overestimate the downward flux of the clear sky because of cloud contamination, marine influence, or inversion, and all are, perhaps, more serious at low temperatures. Third, for a temperature as low as, say, 240 K, the atmosphere should be transparent even in the absorption band, for otherwise the OLR would saturate at a lower temperature than that observed [about 260 K from Fig. 5.16b of Liou (1992)]. The last contention is also supported by Fig. 7.4 of Paltridge and Platt (1976), which shows a vanishing downward flux when the air is comparably dry. While these considerations may justify the use of the model curve, they also underscore its considerable uncertainty.

Given Bo_s and $F_{r,0}$ discussed above and shown in Fig. 3, one may now calculate N_2 from (19), which is also plotted in the figure. As expected from (19), N_2 mimics the curve $1 - F_{r,0}$ (dashed) but is displaced downward where there is a rapid increase of Bo_s^{-1}. This negative correlation between N_2 and $F_{r,0}$ can be explained from the heat balance at level 2 [(12)]. A decrease in $F_{r,0}$, for example, requires an increase in N_2 to block out more of the SW flux to achieve a balance. Somewhat surprising, however, is the muted effect of the latent heat flux in (12) despite the rapid increase of Bo_s^{-1}. This is because the latter effect is countered by vanishing

sensible heat flux in (14), a consequence of vanishing $F_{r,0}$ in (13).

b. High cloud cover

We now proceed to the derivation of the high cloud cover N_3, which is linked to the low cloud cover N_2 through the heat balance at the tropopause,

$$1 - N_2 = (1 - N_3)F_{r,3} + N_3B_3, \tag{21}$$

where $F_{r,3}$ is the clear-sky LW flux and B_3 is the blackbody radiance of the high clouds given by (4). One notes that since the low clouds are emitting at the same temperature as the ocean surface (1), they do not enter the rhs of this equation (the LW flux at the tropopause). Substituting (4) into (21), one derives

$$N_3 = [F_{r,3} - (1 - N_2)][F_{r,3} - (1 - N_2)/2]^{-1}, \tag{22}$$

which allows the calculation of N_3 as a function of the surface temperature once $F_{r,3}$ is specified. Again, a low-order analytical function of the form

$$F_{r,3} = c \tanh(B_0/c) \tag{23}$$

is chosen, which has the requisite property that $F_{r,3} \approx B_0$ toward the low temperature end. The constant c, being the asymptote of the function, represents the maximum OLR (i.e., when the greenhouse effect is saturated), which can be estimated as follows. From satellite observation [see Fig. 5.16b of Liou, (1992)], one may take the maximum emitting temperature in the absorption band to be about 260 K, which has clearly peaked since it is much cooler than the underlying surface (about 320 K). In the spectral window, on the other hand, Hartmann and Michelsen's (1993) curve for the surface LW flux (their Fig. 1) shows that the surface air is rapidly becoming opaque around 300 K, which should give a rough indication of the maximum (outgoing) emitting temperature. Unlike in the absorption band, this temperature is too close to the surface temperature to be discerned from OLR measurements. Given that the two bands compose about 70% and 30%, respectively, of the blackbody radiance, one estimates that $c \approx 0.9$. The resulting $F_{r,3}$ is plotted in Fig. 2, which matches closely the calculated curve of Pierrehumbert (1995, line 4). Using this $F_{r,3}$, I have calculated N_3 from (22), which is plotted in Fig. 3.

To understand the behavior of N_3, let me first rewrite (21) as

$$1 - F_{r,3} = N_2 - N_3(F_{r,3} - B_3). \tag{24}$$

The two terms on the rhs are commonly referred as SW and LW cloud ''forcing'' (Ramananthan and Collins 1991), although such usage has the misleading connotation that clouds constitute external forcing, when they are in fact constrained by internal balances. As seen above, since OLR in the clear sky ($F_{r,3}$) is smaller than the solar flux (of unity)—a consequence of the radiative properties of the water vapor, the lhs is positive: the SW effect of clouds thus necessarily exceeds their LW effect, which can explain the observed net cooling by the global clouds. Another relevant point is that the LW effect of clouds is coupled to their SW effect through the emitting temperature of the high clouds, which, being at the skin temperature, depends on the absorbed SW flux [(4)]. Equation (24) can be combined with (12) to yield

$$N_3(F_{r,3} - B_3) = (F_{r,3} - F_{r,0}) - F_l, \tag{25}$$

which represents the heat balance of the tropospheric layer above the PBL. This equation states that the LW cloud heating on the lhs is balanced on the rhs by the clear-sky cooling of the layer, minus the latent heat flux entering its lower boundary. The increase of the high cloud cover with surface temperature, as depicted in Fig. 3, may now be explained. Since change of the latent heat flux is small, as discussed earlier, the increase in the clear-sky cooling (the greenhouse effect) needs to be balanced by an increasing high cloud cover to block out the OLR.

c. Turbulent wind

The following derivation seeks to link the turbulent wind (at the surface) to the high cloud cover through two essential balances: the water balance that relates the high cloud cover to the volume flux of the deep updrafts and the vapor balance of the PBL that relates this volume flux to the turbulent wind.

As discussed in section 2 (see also Fig. 1), the high clouds result from outflows of the deep updrafts and hence are subjected to water balance of the form (in dimensional units)

$$\frac{d}{da}(V\rho_i) = -w_i\rho_i, \tag{26}$$

where a is the areal coordinate, V is the volume flux of the outflow, and ρ_i and w_i, respectively, are the density and settling velocity of the ''ice'' crystals, the main composition of the high clouds. Since w_i depends on microphysical processes not considered here, it is taken to be an external parameter, independent of the surface temperature. In (26), I have neglected sublimation of the ice crystals, since outflow is typically supersaturated with respect to ice (e.g., Borovikov et al. 1963, chapter VIII). For simplicity, it is assumed furthermore that velocity of the subsiding air is small when compared with that of the falling ice, so that (26) becomes

$$wA\frac{d}{da}\rho_i \approx -w_i\rho_i, \tag{27}$$

in which we have set the volume flux V to that of the updraft as it impinges on the tropopause (with vertical velocity w and area A; see Fig. 1). This equation states simply that the high cloud is dissipated mainly by the gravitational fall out of ice crystals. For lack of better

measures, one may set the high cloud area to the *e*-folding scale in a and nondimensionalize all areas by the global area to yield

$$N_3 = w_i^{-1} wA, \tag{28}$$

which relates the high cloud cover linearly to the volume flux of the updrafts at the tropopause. This volume flux can be equated to that emerging at the LCL (referred as ''core'') based on the following argument. Although air is continuously entrained into or detrained from the updrafts, mixing between the outlying layer and the core is small since the diffusive timescale is long when compared with the transit time of air parcels moving through the updraft (Sun and Lindzen 1993). As such, water condensates that form the high clouds are carried mainly by the core, whose volume flux thus is the relevant one that enters (28).

We next link this volume flux to the turbulent wind at the surface u', which enters the surface flux through the aerodynamic formulas. With the neglect of net condensation in the PBL [see also (5)], the vapor balance of the layer is given by (e.g., Sun and Lindzen 1993)

$$wA(q_1 - q_2) = C_D u'(q_0 - q_1) \tag{29}$$

(where C_D is the drag coefficient). That is, the vapor flux exiting its upper boundary (the LCL) equals the surface evaporation. In (29), I have used the conservation of specific humidity-in the updrafts so that its value at the LCL is the same as the ambient (hence global mean) value at the surface (i.e., q_1). Rearranging (29) yields

$$\frac{C_D u'}{wA} = \frac{q_1 - q_2}{q_0 - q_1}. \tag{30}$$

To express the rhs in terms of the surface temperature, two observational features of the global-mean fields are invoked: one is that the lapse rate is moist adiabatic, as discussed earlier, and the other is that the vapor pressure curve (as a function of temperature) closely parallels the saturation curve [Fig. 3 of Webster (1994)]. The two are not independent, since the latter would imply the former if the saturation moist static energy (or equivalently the equivalent potential temperature) is uniform in height (see appendix C); the latter is also supported by observation (see Fig. 7.6b of PO92). I am not aware of definitive explanations of any of these features, whose uses thus constitute significant empirical elements of the model.

To aid the following derivation, I have sketched in Fig. 4 the (global mean) vapor pressure (thick solid) in the PBL, which, as discussed above, is displaced uniformly from its saturation value (thick dashed), and both are taken to be straight because of the small temperature range spanning the PBL [(1)]. The dotted curve with an arrow traces the rising air in the updrafts, which starts off at the ocean surface temperature T_0 and a vapor pressure e_1. As the air rises, the temperature falls dry adiabatically while the vapor pressure decreases slightly

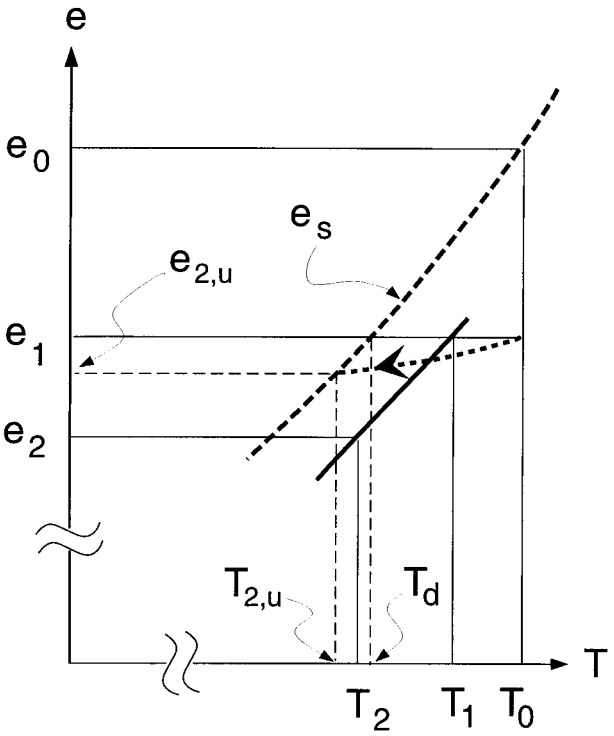

FIG. 4. A schematic of the vapor pressure (thick solid line) as a function of temperature in the PBL, which is parallel to the saturation curve (thick dashed line). Both are taken to be straight because of the small temperature range of the PBL. The dotted curve with an arrow follows the ascending air in the updraft, which intersects the saturation curve at the LCL. Because the slope of the dotted curve is small (as compared with that of the saturation curve), the saturation temperature in the updrafts $T_{2,u}$ equals approximately the dewpoint of the surface air T_d.

because of adiabatic expansion. It reaches saturation at the LCL, with a temperature and vapor pressure subscripted by 2,u (''u'' for ''updraft''). Since the slope of the dotted curve is small when compared with that of the saturation curve (appendix B), one has $e_{2,u} \approx e_1$, and $T_{2,u} \approx T_d$, the dewpoint of the surface air. Given the small pressure difference spanning the PBL on account of (1), the rhs of (30) becomes

$$\frac{q_1 - q_2}{q_0 - q_1} = \frac{e_{2,u} - e_2}{e_0 - e_1}\frac{p_1}{p_2} \approx \frac{e_1 - e_2}{e_0 - e_1} \approx \frac{T_1 - T_2}{T_0 - T_d} \approx \frac{\gamma_m}{\gamma_d}, \tag{31}$$

where γ_m and γ_d are, respectively, the moist- and dry-adiabatic lapse rates that characterize the global-mean temperature and the temperature in the updrafts. As derived in appendix C, the ratio of the two lapse rates is linked to the surface temperature through

$$\frac{\gamma_m}{\gamma_d} = (1 + \mathrm{Bo}_s^{-1})^{-1}, \tag{32}$$

so that a warmer surface, for example, with its smaller (saturation) Bowen ratio would render a smaller moist-adiabatic lapse rate.

Combining (28) and (30)–(32), and nondimensionalizing u' by $C_D^{-1}w_i$, one finally arrives at

$$u' = (1 + \mathrm{Bo}_s^{-1})^{-1}N_3, \tag{33}$$

which links the turbulent wind to the high cloud cover. Although many approximations are used in arriving at this equation, only its gross functional form is seen later to be of significance in determining the model temperature, and its physical content actually is very intuitive. It entails basically that 1) the global high cloud cover, being the outflow of the deep updrafts, is related to evaporation from the surface and 2) this evaporation increases with the turbulent wind and surface temperature. Since the high cloud cover is less than unity, one may already infer from (33) that there is an upper bound on the turbulent wind, or efficiency of the atmospheric heat engine.

With N_3 previously determined, one may now calculate u' from (33), which is plotted in Fig. 3. It is seen that there is a maximum in the turbulent wind, due to the opposing effects of N_3 and Bo_s^{-1} in (33): an increasing surface temperature, for example, implies a more expansive (global) high cloud cover (as explained in section 3b), which acts to strengthen the wind; a warmer surface, on the other hand, is associated with a smaller saturation Bowen ratio, which acts to weaken the wind. With the derivation of (33), one may further justify the use of the saturation Bowen ratio, as alluded to in section 2. This is because an increasing Bowen ratio would increase both N_3 [through (19) and (22)] and the multiplication factor in (33), thus increasing the turbulent wind. The maximization of the latter thus implies that the Bowen ratio is maximized, or approaches its saturation value.

d. Surface temperature

With the hypothesized maximization of the turbulent wind (see section 1), the surface temperature may now be determined from Fig. 3, which has a value of 280 K. To compare with observations, the more relevant variable is the corresponding blackbody radiance, which is seen to be about 10% too low when compared with its modern value. Given the crudeness of the model, it obviously does not distinguish the modern climate, and the above discrepancy is deemed tolerable. Although this temperature is only representative, it is nevertheless significant that even with cloud covers as *free* parameters, the model has produced a surface temperature not unlike the observed one. For other predicted properties, both low and high cloud covers are substantial (45% and 40%, respectively, of the global surface), underscoring their importance in the model. The predicted turbulent wind has a dimensionless magnitude of 0.2. To translate this into a dimensional value, one needs an estimate of the ice-settling velocity. For this, I use the observation of Ackerman et al. (1990), which shows an effective radius of 20–40 μm for ice crystals in cirrus,

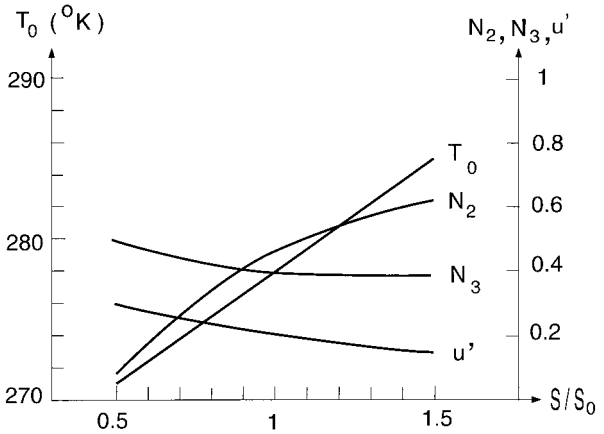

FIG. 5. The model solution for a solar constant S varying by $\pm 50\%$ from its present-day value, S_0. The surface temperature T_0 has changed by 10 K from its present-day value, less than one-third the change in the effective temperature. The heat balances are maintained mainly by internal adjustment of the low cloud cover N_2 that offsets the solar effect. The turbulent wind u' is stronger in the colder climate.

and Fig. 3 of Starr and Cox (1985) to arrive at $w_i \approx 5$ cm s^{-1}. With a drag coefficient of 10^{-3}, the turbulent wind is then 10 m s^{-1}, which is on the right order of the observed magnitude. From (13), the sensible heat flux is estimated to be 0.1, which translates to a dimensional value of 30 W m^{-2}, again on the right order of the observed value. Using the bulk aerodynamic formula and the calculated turbulent wind, one obtains an air–sea temperature difference of about 5 K. Given the assumed lapse rates in the updrafts and in the global-mean temperature and neglecting the inversion strength, one estimates a PBL height of 1 km, which spans a temperature difference of 10 K, in support of the approximation in (1).

Although the specific value of the surface temperature is uncertain, the theory has nevertheless identified robust qualitative bounds, as seen in Fig. 3. The lower bound is associated with the onset of the greenhouse effect (where $F_{r,0}$ decreases rapidly with temperature) and the upper bound is associated with the nonlinear increase of the saturation vapor pressure (and hence Bo_s^{-1}) with temperature. Since both are assumed to be inherent properties of water, one expects the model temperature to be relatively insensitive to changing external conditions. To assess this prediction, I have varied the solar constant by $\pm 50\%$ from its present-day value; the results are shown in Fig. 5. The procedure involves recalculating the curves of Fig. 3 and selecting the solution for which the turbulent wind has a maximum. It is seen that the surface temperature differs from its present-day value by only about 10 K—less than one-third of the change of the effective temperature; the reason that heat balances can be maintained is via the internal adjustment of the low cloud cover that offsets the solar effect. Since this range of the solar constant likely encompasses that which occurred in the geological past,

the theory provides a plausible explanation of an equable climate, so long as there is a *substantial* ocean that allows a full hydrological cycle. The relative insensitivity of the surface temperature to the external forcing, moreover, justifies the many approximations used in the model, since the neglected effects are small when compared with the above change of the solar constant.

The regulatory effects of the low clouds on the climate have been suggested by other regional models (Held et al. 1993; Miller 1997). For observational evidence, one may argue that since life cycles of clouds are short when compared with seasons, cloud covers should be in approximate equilibrium with the seasonal forcing. Based on Fig. 5, one therefore expects low clouds to be more expansive in the summer hemisphere, while high clouds exhibit little seasonal variation. Both these predictions are consistent with the analysis of Hartmann et al. (1992), which may be regarded as an observational support of the theory. Although one is tempted to view the above low cloud effect as a negative feedback, this interpretation is faulty since I have not proposed an independent process—the other half of the feedback loop—that links the low cloud cover to the surface temperature. It is the lack of such linkage that led some researchers (Fu et al. 1992; Pierrehumbert 1995) to question the thermostat hypothesis of Ramanathan and Collins (1991). Because the generation and dissipation of clouds occur on a much shorter timescale than the climate, these processes have little bearing on the climatic cloud cover. In the view of the current theory, the cloud covers merely adjust to whatever is required by global balances, and their regulatory effects enter mainly through the internal degrees of freedom they endow upon the system. In other words, rather than a low cloud that cools the surface, it is the surface temperature—somewhat independently constrained by water properties—that determines the cloud covers through global heat balance. One also expects from Fig. 5 a stronger wind in glacial times, which is consistent with inferences from paleoclimate data (Crowley and North 1991). This agreement could be fortuitous since the model, with all the simplifications, is not intended for addressing such small climate signals.

4. Discussion

To the degree that the model has invoked the observed lapse rate and moisture distribution, it is incomplete and represents only an incremental step from previous models. Its main advances lie in the inclusion of two-level clouds and the turbulent wind as internal variables and, more important, the use of an extremization principle in the model closure. The use of such principles subscribes to the view espoused by many theorists that the climate system is fundamentally underdetermined by macroscopic balances (see section 1). In Webster (1994), such indeterminacy is rooted in the phase change of water, from which he argued that the surface temperature should be near the triple point. In the current model, the inclusion of cloud covers and turbulent wind has provided the needed degrees of freedom, and the surface temperature is again constrained by water properties to be near the triple point. The model, however, has identified specific mechanisms for the bounds through the opposing effects of the greenhouse warming and evaporate cooling on the turbulent wind (as seen in Fig. 3 and discussed in section 3c), a property that is assumed maximized.

To illustrate the difference of this model from that of a deterministic model, let us consider the u' curve in Fig. 3. Prior to its maximization, there is a family of solutions spanning the full range of surface temperature. A deterministic approach would specify u' to obtain a solution, which could be sensitive to the wind chosen—depending on the local slope of the curve or the possibility of jumping to a different branch. Based on the current theory, on the other hand, one chooses the maximum wind, which yields a unique solution of greater stability. In other words, some sensitivity exhibited by deterministic models, such as the runaway scenario of Budyko (1969), could be the artifact of a system unduly stripped of its internal degrees of freedom. By the same token, the theory also points to a possibly major limitation of the GCMs, which are not particularly amenable to dealing with a nondeterministic system.

It should be clear that, since only the state of maximum turbulent wind is realized by the system, the temperature dependence of climate variables depicted in Fig. 3 (thick solid curves) has no counterpart in the observed system and hence may not be used to draw inferences on a changed climate. The latter requires the calculation of a new set of curves from which a maximized solution is selected, which is how Fig. 5 is obtained. Even more trivial, Fig. 3 should *not* be used in any way to infer local correlation between climate variables, since only their global means are subjected to balances that led to the calculation of these curves.

Although the climate variables are calculated over the full range of the surface temperature in Fig. 3, the validity of such calculations obviously is limited by other factors. For example, over the range where the temperature falls below the freezing point, one expects extensive ice to form, which would invalidate the calculation. Although this may not affect the selection of the surface temperature so long as it is above freezing, it poses a limit on climate change calculations as depicted in Fig. 5. That is, if the solar constant is sufficiently low (say, about one-half of its present-day value) that the mean surface temperature falls below freezing point, one may have a very different climate.

Acknowledgments. During the long gestation of the paper, I have benefited from encouragement and comments from many individuals, either after my oral presentations or upon reading early drafts of the paper. The list includes Mark Cane, Tony Del Genio, Adam Sober,

Richard Seager, John Shapiro, and Richard Lindzen. I also thank Jay Fein of the National Science Foundation for his foresight in supporting the work through a SGER Grant ATM-9423233.

APPENDIX A

Maximum Bowen Ratio

We are concerned with the maximum Bowen ratio given a fractional area A_1 of the updrafts. Let the surface temperature of the ''environmental'' air and updrafts be T_e and T_0 (see section 2), respectively; then by definition

$$T_1 = A_1 T_0 + (1 - A_1) T_e. \tag{A1}$$

This equation can be rewritten as

$$T_e = T_0 - \frac{\Delta T}{1 - A_1}, \tag{A2}$$

where $\Delta T \equiv T_0 - T_1$ is the (global mean) air–sea temperature difference, assumed to be small [(1)]. To derive the maximum Bowen ratio, the ambient air is assumed to be saturated, so that

$$e_1 = e_s(T_e). \tag{A3}$$

Substituting (A2) into (A3) and using $e_0 = e_s(T_0)$, one derives

$$e_1 \approx e_0 - \frac{\Delta T}{1 - A_1} \frac{de_s}{dT}, \tag{A4}$$

which can be substituted into (15) to yield

$$\mathrm{Bo}^{-1} = \frac{1}{\gamma} \frac{de_s}{dT} \frac{1}{1 - A_1} = (1 - A_1)^{-1} \mathrm{Bo}_s^{-1}. \tag{A5}$$

APPENDIX B

Vapor Pressure in the Updraft

We want to assess the slope of the thick dashed line in Fig. 4. For an adiabatic ascent, the vapor pressure satisfies

$$\delta e/e = \delta p/p, \tag{B1}$$

since the specific humidity is conserved. Using hydrostatic balance and the equation of state, one has (e.g., Wallace and Hobbs 1977)

$$\delta p/p = -(g/R_d)(\delta z/T), \tag{B2}$$

having neglected the small difference between the temperature and its virtual counterpart (less than 10% over its normal range). With the lapse rate being dry adiabatic in the updrafts, one derives from (B1) and (B2)

$$\delta e/e = (c_p/R_d)(\delta T/T). \tag{B3}$$

Now that the saturation vapor pressure satisfies the Clausius–Clapeyron equation,

$$\delta e_s/e_s = (L/R_v)(\delta T/T^2), \tag{B4}$$

the ratio of (B3) to (B4) gives

$$(\delta e/\delta T)/(\delta e_s/\delta T) = (e/e_s)\Gamma, \tag{B5}$$

where

$$\Gamma \equiv c_p T/0.622L. \tag{B6}$$

For a temperature as high as, say, 300 K, $\Gamma \approx 0.17$, and, with e smaller than e_s, one thus may neglect the slope of the dashed curve relative to that of the saturation curve.

APPENDIX C

Moist-Adiabatic Lapse Rate

I want to derive (32) that links the moist-adiabatic lapse rate to the saturation Bowen ratio. Since a moist-adiabatic lapse rate is equivalent to a uniformity in the saturation moist static energy defined by

$$E = c_p T + gz + Lq_s, \tag{C1}$$

where g is the gravitational acceleration, one may differentiate (C1) with respect to T and set it to zero to yield

$$\frac{\gamma_m}{\gamma_d} = \left(1 + \frac{L}{c_p} \frac{\delta q_s}{\delta T}\right)^{-1}. \tag{C2}$$

With $q_s = 0.622 e_s/p$, the second term in the bracket becomes

$$\frac{L}{c_p} \frac{\delta q_s}{\delta T} = \mathrm{Bo}_s^{-1} \left(1 - \frac{\delta p/p}{\delta e_s/e_s}\right), \tag{C3}$$

where Bo_s is the saturation Bowen ratio given in (17). Using (B2) and (B4), it can be seen that the second term in the bracket is typically small, so that (C2) becomes approximately

$$\gamma_m/\gamma_d = (1 + \mathrm{Bo}_s^{-1})^{-1}. \tag{C4}$$

REFERENCES

Ackerman, S. A., W. L. Smith, J. D. Spinhirne, and H. E. Revercomb, 1990: The 27–28 October 1986 FIRE IFO cirrus case study: Spectral properties of cirrus clouds in the 8–12 μm window. *Mon. Wea. Rev.*, **118,** 2377–2388.

Betts, A. K., and W. Ridgway, 1989: Climatic equilibrium of the atmospheric convective boundary layer over a tropical ocean. *J. Atmos. Sci.*, **46,** 2621–2641.

Borovikov, A. M., I. I. Gaivoronskii, E. G. Zak, V. V. Kostarev, I. P. Mazin, V. E. Minervin, A. Kh. Khrgian, S. M. Shmeter, 1963: *Cloud Physics* (translated from Russian). Israel Program for Scientific Translations Ltd., 392 pp.

Budyko, M. I., 1969: The effect of solar radiation variations on the climate of the earth. *Tellus,* **21,** 611–619.

Cess, R. D., and Coauthors, 1990: Intercomparison and interpretation of climate feed-back processes in 19 atmospheric general circulation models. *J. Geophys. Res.,* **95,** 16 601–16 615.

Clement, A., and R. Seager, 1999: Climate and the tropical oceans. *J. Climate,* **12,** 3383–3401.

Crowley, T. J., and G. R. North, 1991: *Paleoclimatology*. Oxford University Press, 339 pp.

Deardorff, J. W., and J. A. Businger, 1980: Comments on ''Marine stratocumulus convection. Part I: Governing equations and horizontally homogeneous solutions.'' *J. Atmos. Sci.,* **37,** 481–482.

——, G. E. Willis, and D. K. Lilly, 1969: Laboratory investigation of non-steady penetrative convection. *J. Fluid Mech.,* **35,** 7–31.

De Groot, S. R., and P. Mazur, 1963: *Non-Equilibrium Thermodynamics*. North-Holland, 510 pp.

Emanuel, K. A., 1994: *Atmospheric Convection*. Oxford University Press, 580 pp.

Essex, C., 1984: Radiation and the irreversible thermodynamics of climate. *J. Atmos. Sci.,* **41,** 1985–1991.

Fu, R., A. D. Del Genio, W. B. Rossow, and W. T. Liu, 1992: Cirrus-cloud thermostat for tropical sea surface temperatures tested using satellite data. *Nature,* **358,** 394–397.

Garratt, J. R., 1992: *The Atmospheric Boundary Layer*. Cambridge University Press, 316 pp.

Hartmann, D. L., and M. L. Michelsen, 1993: Large-scale effects on the regulation of tropical sea surface temperature. *J. Climate,* **6,** 2049–2062.

——, M. E. Ockert-Bell, and M. L. Michelsen, 1992: The effect of cloud type on the earth's energy balance: Global analysis. *J. Climate,* **5,** 1281–1304.

Held, I. M., and B. J. Soden, 2000: Water vapor feedback and global warming. *Annu. Rev. Energy Environ.,* **25,** 441–475.

——, R. S. Hemler, and V. Ramaswamy, 1993: Radiative–convective equilibrium with explicit two-dimensional moist convection. *J. Atmos. Sci.,* **50,** 3928–3938.

Kondratyev, K. Ya., 1969: *Radiation in the Atmosphere*. Academic Press, 912 pp.

Liou, K. N., 1992: *Radiation and Cloud Processes in the Atmosphere. Theory, Observation, and Modeling*. Oxford University Press, 487 pp.

Lorenz, E. W., 1960: Generation of available potential energy and the intensity of the general circulation. *Dynamics of Climate,* R. L. Pfeffer, Ed., Pergamon Press, 86–92.

——, 1967: *The Nature and Theory of the General Circulation of the Atmosphere*. World Meteorological Organization, Publication No. 218, 161 pp.

Manabe, S., and R. T. Wetherald, 1967: Thermal equilibrium of the atmosphere with a given distribution of relative humidity. *J. Atmos. Sci.,* **24,** 241–259.

Miller, R. L., 1997: Tropical thermostats and low cloud cover. *J. Climate,* **10,** 409–440.

Mobbs, S. D., 1982: Extremal principles for global climate models. *Quart. J. Roy. Meteor. Soc.,* **108,** 535–550.

Paltridge, G. W., 1974: Global cloud cover and earth surface temperature. *J. Atmos. Sci.,* **31,** 1571–1576.

——, 1978: The steady-state format of global climate. *Quart. J. Roy. Meteor. Soc.,* **104,** 927–945.

——, 1979: Climate and thermodynamic systems of maximum dissipation. *Nature,* **279,** 630–631.

——, and C. M. R. Platt, 1976: *Radiative Processes in Meteorology and Climatology*. Elsevier Scientific, 318 pp.

Peixoto, J. P., and A. H. Oort, 1992: *Physics of Climate*. American Institute of Physics, 520 pp.

Pierrehumbert, R. T., 1995: Thermostats, radiator fins, and the local runaway greenhouse. *J. Atmos. Sci.,* **52,** 1784–1806.

Ramanathan, V., and J. A. Coakley Jr., 1978: Climate modeling through radiative–convective models. *Rev. Geophys. Space Phys.,* **16,** 465–489.

——, and W. Collins, 1991: Thermodynamic regulation of ocean warming by cirrus clouds deduced from observations of the 1987 El Niño. *Nature,* **351,** 27–32.

Sarachik, E. S., 1978: Tropical sea surface temperature: An interactive one-dimensional atmosphere–ocean model. *Dyn. Atmos. Oceans,* **2,** 455–469.

Schulman, L. L., 1977: A theoretical study of the efficiency of the general circulation. *J. Atmos. Sci.,* **34,** 559–580.

Starr, D. O., and S. K. Cox, 1985: Cirrus clouds. Part I: A cirrus cloud model. *J. Atmos. Sci.,* **42,** 2663–2681.

Stone, P. H., and J. H. Carlson, 1979: Atmospheric lapse rate regimes and their parameterization. *J. Atmos. Sci.,* **36,** 415–423.

Sun, D. Z., and R. S. Lindzen, 1993: Distribution of tropical tropospheric water vapor. *J. Atmos. Sci.,* **50,** 1643–1660.

Wallace, J. M., and P. V. Hobbs, 1977: *Atmospheric Science*. Academic Press, 467 pp.

Webster, P. J., 1994: The role of hydrological processes in ocean–atmosphere interactions. *Rev. Geophys.,* **32,** 427–476.